Phosphorescent Carbene-Gold-Arylacetylide Materials as Emitters for Near UV-OLEDs

Alexander C. Brannan, Hwan-Hee Cho, Antti-Pekka M. Reponen, Mikko Linnolahti,* Manfred Bochmann,* Neil C. Greenham,* and Alexander S. Romanov*

A series of carbene-gold-acetylide complexes $[(BiCAAC)AuCC]_nC_6H_{5-n}$ ($n = 1$, Au1; $n = 2$, Au2; $n = 3$, Au3; BiCAAC = bicyclic(alkyl)(amino)carbene) have been synthesized in high yields. Compounds Au1–Au3 exhibit deep-blue to blue-green phosphorescence with good quantum yields up to 43% in all media. An increase of the (BiCAAC)Au moieties in gold complexes Au1–Au3 increases the extinction coefficients in the UV–vis spectra and stronger oscillator strength coefficients supported by theoretical calculations. The luminescence radiative rates decrease with an increase of the (BiCAAC)Au moieties. The time-dependent density functional theory study supports a charge-transfer nature of the phosphorescence due to the large (0.5–0.6 eV) energy gap between singlet excited (S_1) and triplet excited (T_1) states. Transient luminescence study reveals the presence of both nonstructured UV prompt-fluorescence and vibronically resolved long-lived phosphorescence 428 nm. Organic light-emitting diodes (OLED) are fabricated by physical vapor deposition with 2,8-bis(diphenylphosphoryl)dibenzo[b,d]furan (PPF) as a host material with complex Au1. The near-UV electroluminescence is observed at 405 nm with device efficiency of 1% while demonstrating OLED device lifetime LT_{50} up to 20 min at practical brightness of 10 nits, indicating a highly promising class of materials to develop stable UV-OLEDs.

1. Introduction

Organic light-emitting diodes (OLEDs) are now ubiquitous in commercial devices for display and lighting technologies, as well as others. However, despite the considerable amount of research that has been devoted to red, green, and blue OLEDs, ultraviolet-emitting OLEDs (UV-OLEDs) remain elusive, with only a few examples reported to date. Current UV sources mainly comprise of UV-LEDs and UV mercury lamps.[1] OLEDs have many advantages over such legacy lighting technologies, such as flexible and large array displays, as well as being free of mercury.[2,3] UV light sources are desirable for a range of timely and important application areas, such as sterilization and disinfection of pathogens, water purification, modern agriculture, and anticounterfeit detection.[3–7] Despite the immense potential of UV-OLEDs, only a small number of those are described thus far, indicating difficulty in preparing stable devices due to high-energy required to create UV-photons that eventually results in a degradation of the light-emitting material and poor device lifetimes which are rarely reported in the literature.[8–10] The most recent high efficiency near-UV OLED was reported to reach up to 10% maximum external quantum efficiency (EQE),[11] however, it experience a significant roll-off down to 6% already at practical brightness of 10 cd m^{-2} thus indicating the complexity of the problems associated with near-UV OLED stability.

To make UV-OLEDs feasible, a stable emitter with a short radiative lifetime is required to reduce degradation and adverse

A. C. Brannan, A. S. Romanov
Department of Chemistry
The University of Manchester
Oxford Rd., Manchester M13 9PL, UK
E-mail: alexander.romanov@manchester.ac.uk

H.-H. Cho, A.-P. M. Reponen, N. C. Greenham
Department of Physics
Cavendish Laboratory
Cambridge University
Cambridge CB3 0HF, UK
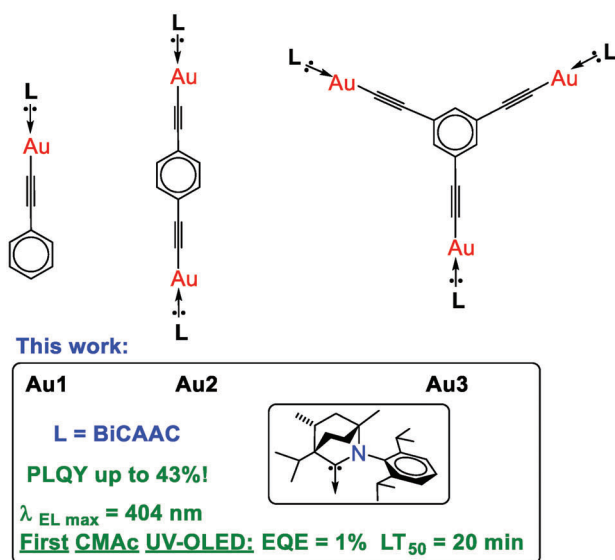E-mail: ncg11@cam.ac.uk

M. Linnolahti
Department of Chemistry
University of Eastern Finland
Joensuu FI-80101, Finland
E-mail: mikko.linnolahti@uef.fi

M. Bochmann
School of Chemistry
University of East Anglia
Earlham Road, Norwich NR4 7TJ, UK
E-mail: m.bochmann@uea.ac.uk

L = PPh₃, Yam et al., 1996 [16]
L = PCy₃, Che et al., 2002 [17]
$\lambda_{\text{emission max}}$ = 421–491 nm (solid)
τ = 33–96 µs
PLQY 3–22%

L = NHC: Nolan et al., 2010 [18]
$\lambda_{\text{emission max}}$ = 439–496 nm (solid)
τ = not reported
PLQY <1%

L = BenzNHC: Venkatesan et al., 2012 [19]
$\lambda_{\text{emission max}}$ = 424 nm (CH₂Cl₂)
τ = 0.7 µs
PLQY <1%

L = PyrNHC: Chen et al., 2022 [21]
$\lambda_{\text{emission max}}$ = 435 nm (solid)
τ = 51 µs
PLQY 36%

This work:

Au1   Au2   Au3

L = BiCAAC
PLQY up to 43%!
$\lambda_{\text{EL max}}$ = 404 nm
First CMAc UV-OLED: EQE = 1% LT₅₀ = 20 min

Scheme 1. Gold complexes **Au1–3**.

reactions within the device. Recently, carbene-metal-amide (CMA) emitters have emerged as promising Au(I) complexes for application in OLEDs, enabling devices with up to 26% external quantum efficiency (EQE) at practical brightness of 100 nits.[12] CMA materials are two-coordinate coinage metal complexes, where the metal is coordinated with a neutral carbene and an anionic amide ligand. To prepare more stable emitters, one needs to consider the organometallic complex with a more covalent bond character between the gold atom and the ligands, thus increasing bond dissociation energy for a less polarized chemical bond. Therefore, we considered exchanging the anionic amide ligand in CMA with a carbon-based (aryl)acetylide ligand due to similar values in electronegativity (≈2.5)[13] for gold and carbon atoms. For over two decades, various cyclometallated Au(III)-(aryl)acetylide complexes have been thoroughly investigated and applied in electroluminescent devices to produce sky-blue, green, and red OLEDs.[14,15] Also, Au(I)-(aryl)acetylide complexes are one of the most stable organogold compounds with well-reported photophysical behavior in the literature but are hardly applied in OLED devices. One of the plausible explanations could be a relatively long excited state lifetime (10–100 ms) and poor luminescence quantum yields. In **Scheme 1**, we assembled a chronological evolution of the ligated Au(I)-(aryl)acetylide complexes and their performance. For instance, the luminescence efficiency increases with an increase in the σ-donor property of the neutral lignad when comparing (L)Au(C≡CPh) complexes where L = PPh₃ (Ph = phenyl, poor photoluminescence quantum yield (PLQY))[16] and PCy₃ (Cy = cyclohexyl, PLQY up to 22%).[17] Nolan[18] and Venkatesan[19] reported various (L)Au(C≡CPh) complexes (Scheme 1), where L is one of the conventional N-heterocyclic carbene ligands. These mononuclear complexes are practically nonemissive in the solid state (PLQY values are ≈1%, Scheme 1), whereas di- and multinuclear complexes may show enhanced PLQY values (up to 30%) due to the
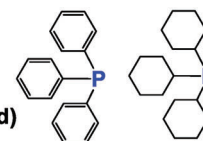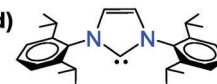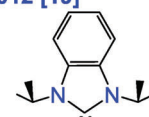
aurophilic (Au···Au) interactions.[20] Chen et al. recently reported alkynyl complexes (L)Au(C≡C-Aryl)[21] where L is a pyrazine-fused NHC-carbene having stronger π-accepting properties compared with conventional NHC-carbenes (Scheme 1). This molecular design resulted in various complexes to have either blue phosphorescence (PLQY 36%) or bright green and yellow thermally activated delayed fluorescence (TADF with PLQY up to 76%) emitters while demonstrating green and yellow OLEDs with up to 9.7% EQE at practical brightness of 1000 cd m⁻².[21]

Here we investigated a series of carbene-metal-acetylides (CMAc) complexes $\{(\text{BiCAAC})\text{AuCC-}\}_n\text{C}_6\text{H}_{6-n}$ as shown in Scheme 1 ($n = 1$ for **Au1**, 2 for **Au2**, and 3 for **Au3**). Unlike previous works (Scheme 1), we decided to use a bicyclic(alkyl)(amino)carbene (BiCAAC) ligand with superior σ-donor and π-acceptor properties compared to phosphine and conventional NHC-carbene ligands. Complexes **Au1–Au3** are investigated to ascertain the effect of multiple gold atoms on the photophysical properties of the emitters. Unlike complexes with conventional NHC ligands, the mono-substituted complex (**Au1**) shows the most suitable and bright phosphorescence with PLQY up to 43%. **Au1** reveals a high-energy fast, prompt fluorescence ¹($\pi\pi^*$) as well as a long-lived phosphorescence ³($\pi\pi^*$), where the latter can be quenched by a suitable host material in the emitting layer of the OLED. By quenching the triplet emission, for instance, by using DPEPO host material for the emitting layer, we exclusively see prompt fluorescence in the OLED devices, resulting in near-UV electroluminescence of 1% and excellent device operational stability of 20 min (LT₅₀).

2. Results and Discussion

Gold complexes **Au1–3** (Chart 1) were prepared in high yields by reaction of (BiCAAC)AuCl[22] with KO^{t}Bu and ethynylbenzene (**Au1**), 1,4-diethynylbenzene (**Au2**), or 1,3,6-triethynylbenzene

**ADVANCED
SCIENCE NEWS**

www.advancedsciencenews.com
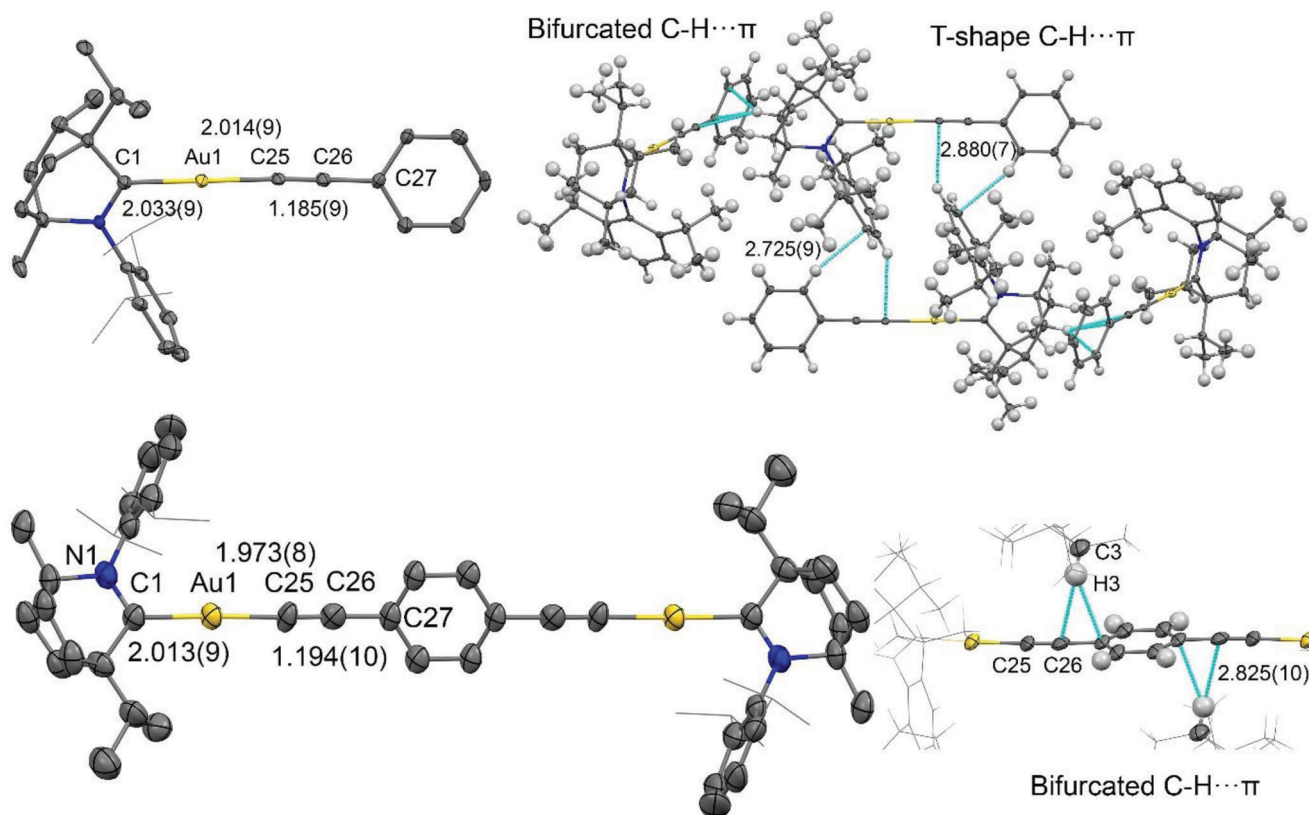
**ADVANCED
MATERIALS**

www.advmat.de

Figure 1. Crystal structures (left) and intermolecular contacts (right) for gold complexes Au1 (top) and Au2 (bottom) with key geometrical parameters. Ellipsoids are shown at the 50% level.

(**Au3**), respectively. All gold complexes are off-white solids soluble in toluene and polar aprotic solvents (dichloromethane and tetrahydrofuran) and stable for several months in the solid state in air. The carbene–carbon resonances exhibit minor deviation from 261.6 ppm (±0.1) in ^{13}C NMR spectra for **Au1–3**, indicating similar chemical and electronic environments for the (Bi-CAAC)Au moiety. The characteristic IR absorption band for C≡C triple bond is measured at ≈2110 cm^{-1} for **Au1–Au3** complexes, which is closely similar to various gold compounds with arylacetylide ligands.[16–20,23] Thermogravimetric analysis has been used to determine the decomposition temperature (T_d, 5% mass loss as shown in Figure S1, Supporting Information), indicating lower thermal stability for the monogold complex **Au1** (297 °C) compared with **Au2** (342 °C) and **Au3** (331 °C). Regardless of lower thermal stability for **Au1**, it was successfully sublimed on a gram scale at 210 °C and 5×10^{-6} mbar pressure to obtain high purity samples for the fabrication of the OLED devices, vide infra.

Crystals of **Au1** and **Au2** suitable for X-ray diffraction were obtained by layering CH_2Cl_2 solutions with hexane. The molecular structures and key geometric parameters are collected in **Figure 1**, together with key intermolecular contacts. All compounds are monomeric with no close aurophilic interactions between the gold atoms. Both **Au1** and **Au2** exhibit linear geometry around the gold atom with an identical C1–Au–C25 angle of 176.7(4)°. Both the gold–carbene(C1) and gold–acetylide(C25) bond lengths are shorter by 0.02–0.04 Å for the digold complex **Au2** compared

with mononuclear **Au1**. Such deviations in bond lengths result in 0.06(1) Å longer carbene(C1)⋯acetylide(C25) distance for the compound **Au1**. The acetylide C25≡C26 triple bond length is slightly longer for the **Au2** compared with **Au1**, however, the deviation is within the experimental error of 0.01 Å.

Intermolecular contacts have been analyzed for compounds **Au1** and **Au2** to gain more insight into measured gold—carbon bond length deviations. The neighboring molecules are arranged into 3D networks by weak hydrogen bonds between soft C—H acids and soft π-bases (double, triple, and aromatic moieties), as shown in Figure 1. Complex **Au2** exhibits a bifurcated hydrogen bond where C3—H3(carbene) is pointed to the center of the C26$_{(C≡C)}$—C27$_{(phenyl)}$ bond (Figure 1). This results in 0.04 Å elongation of the C26—C27 bond for **Au2** compared with **Au1**, where a similar hydrogen bond C6—H6(carbene) is formed with three sp^2-hybridized carbons (C26, C27, and C32), resulting in much smaller bond elongation (0.02 Å for C26—C27 and C27—C32) due to better delocalization for **Au1**. Unlike **Au2**, complex **Au1** exhibits a short T-shape hydrogen bond C16—H16 pointed toward the acetylide terminal carbon atom C25 which is attached to a gold atom Au1. This fact corroborates the 0.06 Å longer gold—acetylide bond length for **Au1** compared with **Au2** due to the weakening of the bonds attached to the somewhat more electron-deficient C25 carbon atom participating in a weak hydrogen bonding.

Cyclic voltammetry was performed in THF solutions, with data summarized in **Table 1**. Combined cyclic voltammograms are

**ADVANCED
SCIENCE NEWS**

www.advancedsciencenews.com

**ADVANCED
MATERIALS**

www.advmat.de

Table 1. Formal electrode potentials (peak position E_p for irreversible and $E_{1/2}$ for quasireversible processes (*), V, vs FeCp$_2$), onset potentials (E, V, vs FeCp$_2$), peak-to-peak separation in parentheses for quasireversible processes (ΔE_p in mV), E_{HOMO}/E_{LUMO} (eV) and bandgap values (ΔE, eV) for the redox changes exhibited by complexes **Au1–3**.

Complex[a]	Reduction		E_{LUMO} [eV]	Oxidation		E_{HOMO} [eV]	ΔE [eV]
	$E_{1/2}$	$E_{onset\ red}$		E_P	$E_{onset\ ox}$		
Au1	−2.87* (162)	−2.78	−2.61	+0.95	+0.71	−6.10	3.49
Au2	−2.87* (228)	−2.77	−2.62	+0.65	+0.47	−5.86	3.24
Au3	−2.93* (323)	−2.79	−2.60	+0.86	+0.59	−5.98	3.38

[a] In THF solution, recorded using a glassy carbon electrode, concentration 1.4 mM, supporting electrolyte [n-Bu4N][PF6] (0.13 M), measured at 0.1 V s^{-1}. E_{HOMO} = −($E_{onset\ ox}$ Fc/Fc+ + 5.39) eV; E_{LUMO} = −(E onset red Fc/Fc+ + 5.39) eV.[24]

shown in **Figure 2**. Complexes **Au1–3** show a quasireversible reduction process at −2.90 ± 0.03 V with little variation in $E_{1/2}$. This value is closely similar to the previously reported CMA1 (^{Ad}CAACAuCz) complex.[12] The quasireversibility of the reduction peak can be demonstrated by the increase in the peak-to-peak separation values ΔE_p from 162 to 323 mV (at 100 mV s^{-1}) for **Au1–Au3**, which deviates from the ideal value of 59 mV for a one-electron reversible couple (Table 1). The reduction wave for complexes **Au1–Au3** exhibits the ratio between cathodic and anodic currents i_{pc}/i_{pa} in the range of 0.73–0.85, somewhat deviating from the ideal unity value for the fully reversible couple. Both cathodic and anodic currents experience concurrent increase with the number of the (BiCAAC)Au moieties in complexes **Au1–Au3**, implying that the LUMO (−2.61 ± 0.01 eV) is largely localized on the (BiCAAC)Au moiety for all complexes. Oxidation of the compounds **Au1–Au3** results in an irreversible wave with no reduction back-peak. Significant variation in E_p values was measured, 0.59 ± 0.12 V, thus indicating the HOMO is largely localized on the arylacetylide of the compounds. The change in E_p demonstrates that the energy of the HOMO varies with the number and position of the (BiCAAC)Au-C≡C moieties on the central benzene ring (Figure 2 and Table 1). This affects the energy gap values, which increase in the order of **Au2** (3.24 eV) < **Au3** (3.38 eV) < **Au1** (3.49 eV).

2.1. Photophysical Properties and Theoretical Considerations

The UV–vis spectra for all complexes are shown in **Figure 3** (Figure S3a,b, Supporting Information), while the photophysical parameters are collected in **Table 2** in various media. The UV–vis spectra show a broad and weakly-resolved absorption band in the 300–375 nm region, see Figure 3a. This band experiences a 40 nm blueshift with an increase in the solvent polarity (Figure 3b), thus demonstrating a negative solvatochromism similar to carbene-metal-amide materials.[12] The energy gap values between the highest occupied and lowest unoccupied electronic levels were estimated from the red onset of the lowest-in-energy absorption band in the UV–vis spectra in THF solution for all gold complexes (3.57 eV for **Au1**, 3.28 eV for **Au2**, and 3.42 eV for **Au3**). The values correlate with the energy gap calculated from the electrochemistry experiment in THF, indicating luminescence for monogold complex **Au1** to be more blueshifted, whereas being redshifted for complex **Au2**.

We ascribe the lowest-energy bands to a metal-mediated charge-transfer (L(M)LCT) from arylacetylide (HOMO) to carbene (LUMO) in line with our theoretical calculations, see **Figure 4**. The lowest-energy bands of monogold compound **Au1** possess a molar extinction coefficient of ≈1×10^4 M^{-1} cm^{-1}, while di- and trigold complexes **Au2–3** show molar extinction coefficients of ≈4 × 10^4 M^{-1} cm^{-1}, thus indicating a higher allowance of the excitation when increasing the number of (BiCAAC)Au(acetylide) moieties. Theoretical calculations support this experimental fact with higher oscillator strength coefficients for the S$_0$→S$_1$ transition in the case of the digold complex **Au2** (f = 1.3447; f = 0.7947 for **Au3**) compared with monogold complex **Au1** (f = 0.4426). Such increases in the UV–vis extinction coefficients have been observed before for the organometallic and organic TADF materials.[25,26] For instance, Wright et al. demonstrated that the increase of the spatial overlap of the molecular orbitals or homoconjugation enhances the photophysical properties of the materials by facilitating an intramolecular charge-transfer process when compared to the classic donor–acceptor systems.[25]

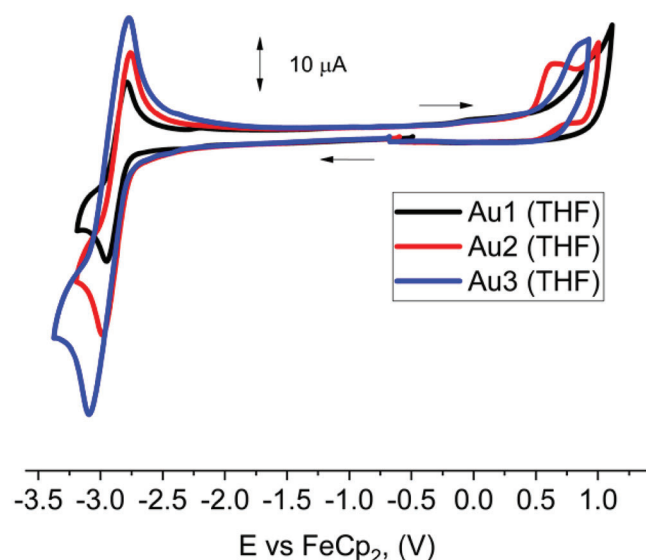

Figure 2. Full range cyclic voltammogram of complexes **Au1–3**. Recorded using a glassy carbon electrode in THF solution (1.4 mM) with [n-Bu$_4$N]PF$_6$ as supporting electrolyte (0.13 M), scan rate 0.1 V s^{-1}.
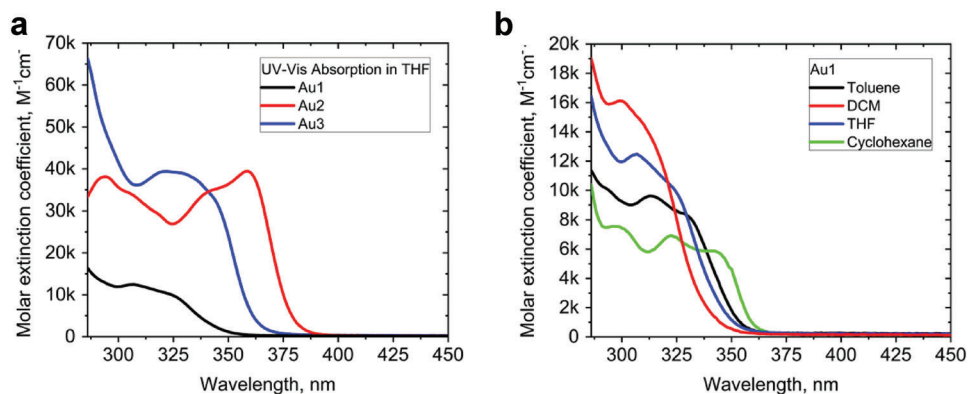
Figure 3. a) UV–vis spectra of complexes **Au1–3** in THF at 295 K. b) UV–vis spectra of complex **Au1** in various solvents at 295 K.

Indeed, theoretical calculations show an increase in the degree of the homoconjugation between HOMO and LUMO orbitals reflected by the increase of the HOMO-LUMO overlap integrals for the gold complexes: 0.42 for **Au1** and 0.47 for **Au2**. This clearly illustrates that greater homoconjugation in **Au2** leads to an enhancement in the extinction coefficient of the CT band.[25] Complex **Au3** shows no significant trend since the $S_0 \rightarrow S_1$ transition corresponds to largely a combination of the HOMO-LUMO

(20%), HOMO–1-LUMO+1 (20%), and HOMO–1-LUMO+2 (36%) transitions (Table S2, Supporting Information). The isosurfaces and overlap integrals for the pertinent orbitals of the trigold complex (**Au3**) indicate a somewhat smaller homoconjugation compared with the digold complex (**Au2**), explaining a slightly lower enhancement of the extinction coefficients regardless of the larger number of the (BiCAAC)Au(acetylide) moieties.

Table 2. Photophysical properties of all complexes.

	λ_{em} [nm]	τ [μs]	Φ [%][a]	k_r [10^3 s^{-1}][b]	k_{nr} [10^3 s^{-1}][c]	T_1 [eV][d]	λ_{em} [nm, 77 K]	τ [μs, 77 K]
Toluene solution							Frozen MeTHF solution	
Au1	429	24.2	27	11.2	30.2	2.99	424	149.7
Au2	502	77.3	27	3.49	9.44	2.54	492	182.6
Au3	455	47.6	21	4.41	16.6	2.81	447	494.8
2 wt% PS matrix								
Au1	429	73.1 (58%), 112.6 (42%)	16	1.78	9.37	2.96	427	92.5 (82%), 148.0 (18%)
Au2	501	30.5 (40%), 80.9 (60%)	10	1.65	14.8	2.52	504	43.1 (23%), 128.1 (77%)
Au3	453	8.2 (19%), 208.3 (81%)	6	0.352	5.52	2.84	446	58.1 (18%), 247.6 (82%)
20 wt% DPEPO matrix								
Au1	428	60.4 (30%), 121.7 (70%)	43	4.16	5.51	2.98	426	121.2 (94%), 256.4 (6%)
Au2	500	75.7 (18%), 148.0 (82%)	37	2.74	4.67	2.54	499	120.0 (47%), 180.5 (53%)
Au3	452	64.2 (30%), 330.1 (70%)	22	0.879	3.12	2.78	453	108.6 (17%), 419.7 (83%)

[a] Quantum yields determined using an integrating sphere; [b] Radiative rate constant $k_r = \Phi / \tau$; [c] Nonradiative constant $k_{nr} = (1 - \Phi) / \tau$. In case of two-component lifetime τ an average was used: $\tau_{av} = (B_1/(B_1 + B_2))\tau_1 + (B_2/(B_1 + B_2))\tau_2$, where B_1 and B_2 are the relative amplitudes for τ_1 and τ_2, respectively; [d] T_1 energies based on the onset values of the emission spectra blue edge in MeTHF glasses at 77 K.

**ADVANCED
SCIENCE NEWS**
www.advancedsciencenews.com

**ADVANCED
MATERIALS**
www.advmat.de

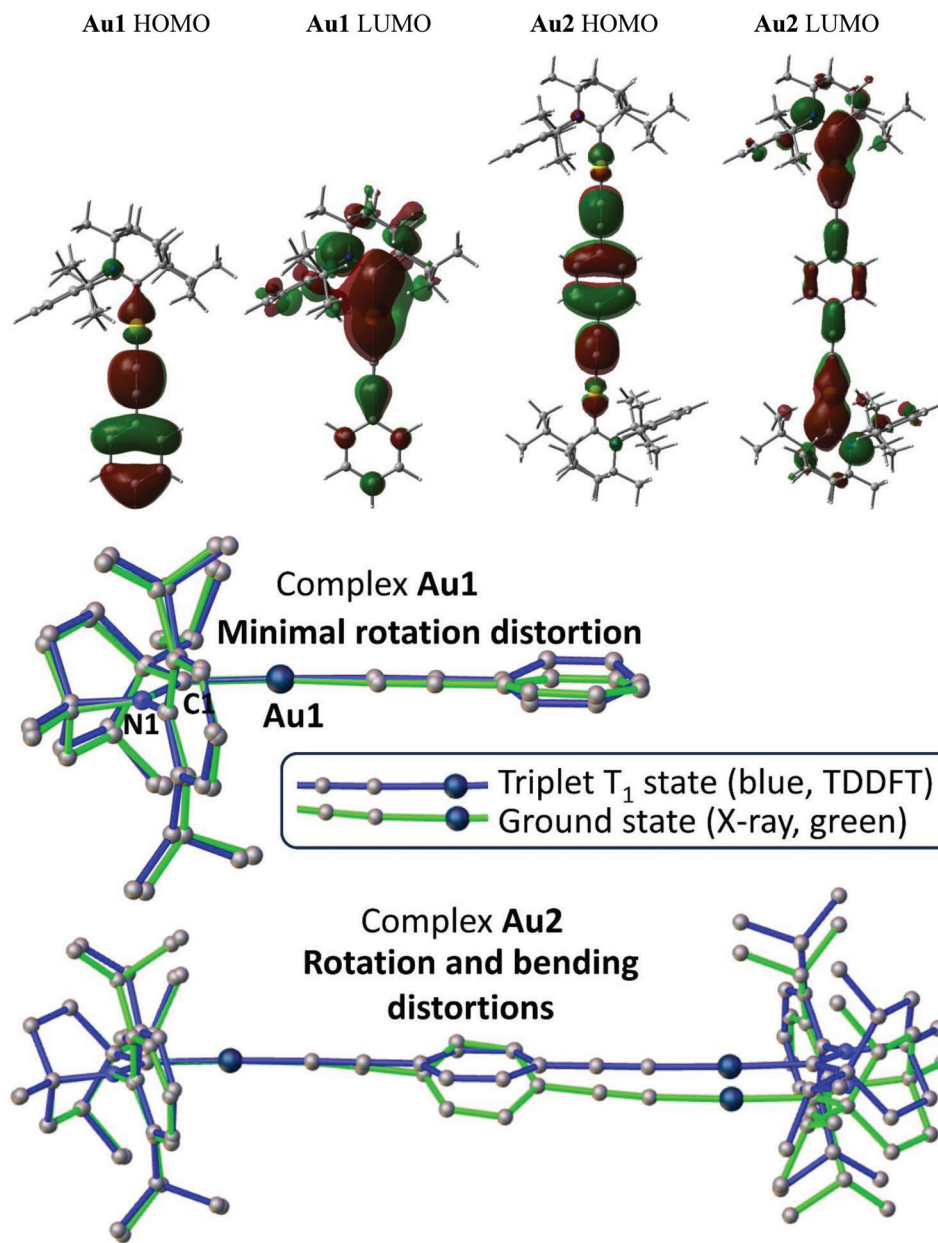**Au1** HOMO   **Au1** LUMO   **Au2** HOMO   **Au2** LUMO

Figure 4. Top: HOMO and LUMO plots of **Au1** (left) and **Au2** (right). Bottom: superposition of the crystal structure (green) and excited triplet T_1 (blue) geometries for complexes **Au1** and **Au2** (overlay via C1, C2, and N1 atoms) determined by theoretical calculations and showing rotational and bending distortions.

The photoluminescence (PL) spectra for all complexes are shown in **Figure 5**, while the photophysical parameters are collected in various media and presented in Table 2. The steady-state emission of complexes **Au1**–**Au3** in all media shows an acetylide-centered and vibronically resolved $^3(\pi\pi^*)$ phosphorescence profile with peak PL at 429 nm (**Au1**), 505 nm (**Au2**), and 455 nm (**Au3**). Complexes **Au2** and **Au3** demonstrate 26–76 nm redshift of the PL profiles compared with **Au1**, which results from the perturbation produced by increasing the number of the gold atoms coordinated with the acetylide core ligand.[27] Gold complexes **Au1**–**Au3** demonstrate only minor solvatochromism (up to 5 nm) in various media and solvents of different polarities (see Figure 5;

and Figure S4, Supporting Information). The trend of λ_{em} values of **Au1**–**3** follow the bandgap energies measured by cyclic voltammetry and UV–vis spectroscopy, see above, as well as TD-DFT calculations (Table S5, Supporting Information), where **Au1** shows a deep-blue emission, **Au2** shows a green emission, and **Au3** shows a blue emission in all media. Moreover, a highly-resolved PL profile remains intact upon freezing the solution and films down to 77 K (Figure 5), indicating an acetylide-centered $^3(\pi\pi^*)$ PL with a similar nature at room and 77 K temperature.

To confirm the nature of the phosphorescence nature of the PL, we measured the excited state lifetimes for all gold complexes at 295 and 77 K (see Table 2). At room temperature, all complexes
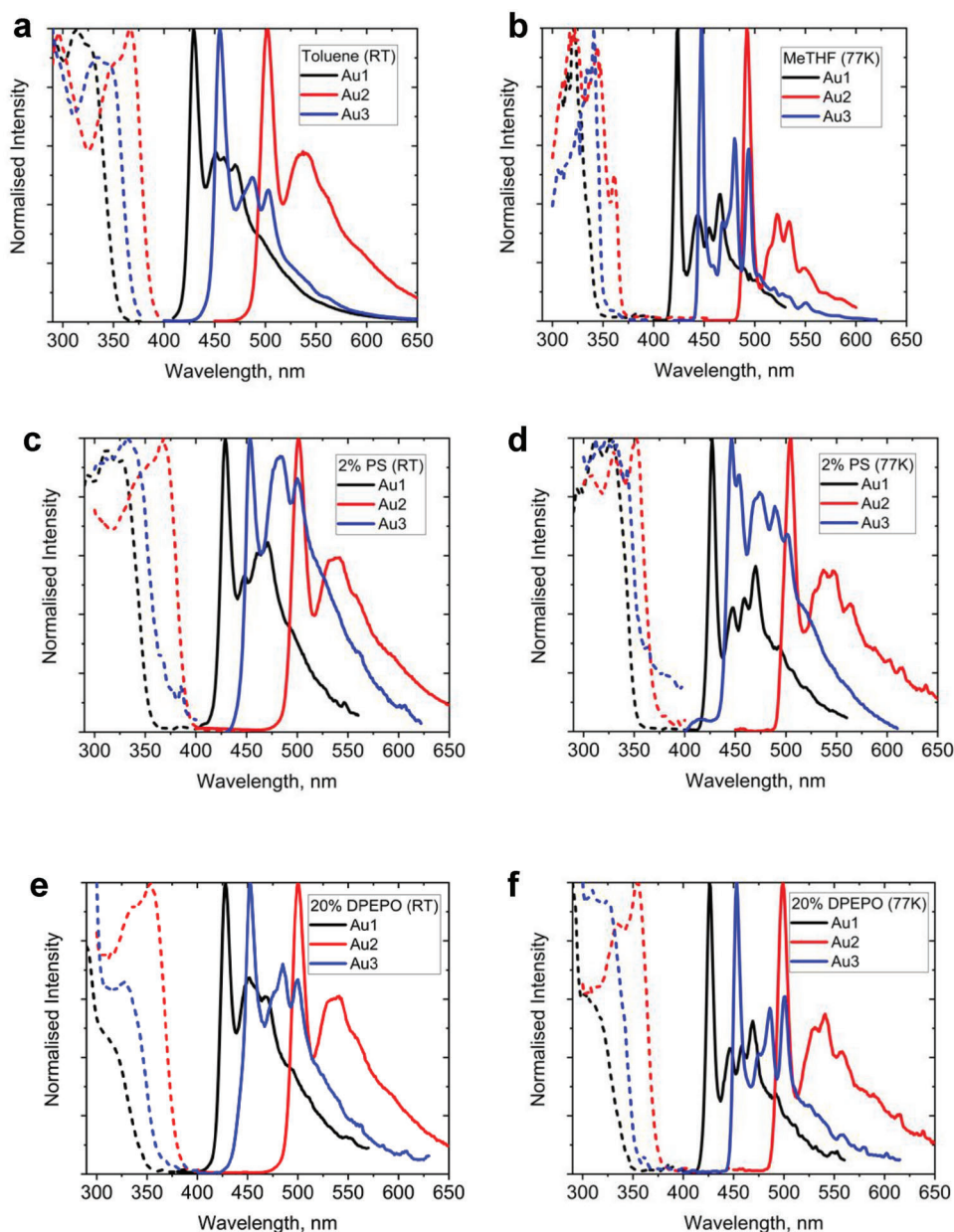
**ADVANCED
SCIENCE NEWS**

www.advancedsciencenews.com

**ADVANCED
MATERIALS**

www.advmat.de

Figure 5. Photoluminescence spectra (solid line) and excitation spectra (dashed line) of **Au1**–**3** in various media. a) Toluene solutions (295 K). b) MeTHF frozen solutions (77 K). c) Polystyrene 2wt% films (295 K). d) Polystyrene 2 wt% films (77 K). e) DPEPO 20 wt% films (295 K) and f) DPEPO 20 wt% films (77 K).

demonstrate long excited state lifetimes in the range of 24–80 µs (with biexponential PL decays), and the values increase with the number of the (BiCAAC)Au moieties from **Au1** to **Au3**. We measured a nearly twofold increase of the excited state lifetime upon cooling to 77 K, thus enabling us to assign the nature of the PL to phosphorescence from the acetylide triplet intraligand excited state (^{3}IL(C≡C)) and facilitated by the large spin–orbit coupling from the Au(I) atom. Complex **Au1** in a 2% PS host shows only a marginal increase for the excited state lifetime on cooling from 296 to 16 K (Figure S4, Supporting Information). The phosphorescence profile attains a more vibronically resolved structure at 16 K (varied temperature experiment as shown in Figure S4, Sup-

porting Information), thus further supporting the assignment of the phosphorescence and ruling out TADF.

Our theoretical calculations (Table S6, Supporting Information) reveal a different conformation between the planes of the BiCAAC carbene and phenylacetylide ligands for S_1 (twisted) and T_1 (nearly coplanar like S_0) excited state geometry for **Au1–2**. We calculated the large energy difference between S_1 and T_1 excited state of ≈0.6 eV for **Au1–3** (see Figure 5; and Table S5, Supporting Information). This result correlates well with the theoretically calculated larger overlap integral between HOMO and LUMO orbitals ($O_{H/L}$) for these complexes; for instance, $O_{H/L} = 0.47$ for **Au2** is larger than 0.36 for the archetype CMA1 complex.[12] The

**ADVANCED
SCIENCE NEWS**

www.advancedsciencenews.com

**ADVANCED
MATERIALS**

www.advmat.de

larger the $O_{H/L}$, the greater the stabilization of the T_1 state for the phosphorescent materials. Since the S_0-S_1 transition character is predominantly HOMO-LUMO (85% and 91% for **Au1** and **Au2**, respectively), we expect the initial photoexcitation to populate the ^{1}CT state, followed by rapid intersystem crossing ISC to a ^{3}CT state and then nonradiative relaxation to the lowest in energy intraligand ^{3}IL($\pi\pi^*$) state demonstrating a vibronically resolved phosphorescence.

Lifetimes in films are fitted biexponentially and in solution monoexponentially. A marked increase in lifetimes in both solution and films on cooling from 295 to 77 K indicates quenching of phosphorescence at 295 K by a nonradiative process. Despite this, complexes **Au1–3** show high phosphorescent quantum yields of 43%, 37%, and 22%, respectively, in 20% DPEPO films at 295 K. In polystyrene (PS) and DPEPO films, the lifetimes of the complexes increase with the number of gold units (103, 135, and 250 µs for **Au1**, **Au2**, and **Au3**, respectively, in 20% DPEPO films at 295 K). The highest PLQYs are measured in the DPEPO host and decrease from **Au1** (up to 43%) to **Au2** (up to 37%) and **Au3** (up to 22%, Table 2). The PLQY for the **Au1** phosphorescence is one of the highest reported to date for mononuclear (carbene)Au(I)(phenylacetylides) that are not enhanced by aurophilic interactions. Therefore, the radiative rates decrease with an increase in the number of (BiCAAC)Au units and indicate that distortion of the linear geometry in the excited state is more likely for the larger complexes, i.e., **Au3**, thus outcompeting any benefits gained by increasing the heavy-atom effect with multiple (BiCAAC)Au-C≡C moieties. In fact, the toluene solution for **Au3** shows shorter lifetimes than **Au2** (47.6 and 77.3 µs for **Au3** and **Au2**, respectively). This is likely a result of increased nonradiative decay in solution due to a larger number of (BiCAAC)Au moieties and, therefore, a greater number of possible nonradiative pathways present in a fluid medium than compared to a rigid medium such as film or frozen solution.

To reveal the distortions responsible for the nonradiative processes, we overlayed the molecular coordinates from the X-ray single crystal diffraction experiment and calculated coordinates for the triplet excited state (T_1) for phosphorescent complexes **Au1** and **Au2** (Figure 4). Complex **Au1** has only minor 10° rotational distortion whereas complex **Au2** experiences a severe out of plane bending and rotation of the phenyl(alkynyl) moiety which occurs upon photoexcitation as shown in Figure 4. Such bending and rotational distortions are likely responsible for the gradual decrease in PLQY with increase of the (BiCAAC)Au moieties for **Au1** to **Au3** (see Table 2). Given such severe distortions for **Au2**, this problem will be even more pronounced for complex **Au3**, which has the highest number of the (BiCAAC)Au moieties and the lowest PLQY values in the series. Such Renner–Teller type distortions are associated with the bending in the linear fragment and were discussed previously for another class of carbon-based emitters—Carbene-Au(I)-Aryls.[28]

2.2. Transient Emission and Absorption Spectroscopy

Next we measured transient luminescence and absorption kinetics for the CMAc complexes **Au1–Au3**, where the most bright acetylide complex, **Au1**, was considered in more detail to gain more insights about its luminescence nature. The transient PL kinetic profile for polystyrene (PS) film of **Au1** (**Figure 6**a) has been probed at several time domains. Early time regime (up to 5 ns) for **Au1** shows a high energy fluorescence with unstructured profile peaking at 410 nm (Figure 6b, brown profile). We ascribe this luminescence to the singlet charge transfer state ^{1}CT (HOMO→LUMO, **Scheme 2**). The PS films and toluene solutions of complexes **Au2** (Figure S6, Supporting Information) and **Au3** (Figure S7, Supporting Information) possess similar featureless and broad CT prompt fluorescence with up to 30 nm redshift compared with **Au1**. Next we analyzed profiles (Figure 6b) from a submicrosecond regime (red profile) and after a delay of 10 µs (orange) and 100 µs (yellow). The red PL profile in the submicrosecond regime (10–100 ns) demonstrates a well-resolved vibronic structure (Figure 6b) which is very similar to the highly-resolved PL profile measured for **Au1** at 16 K (Figure 6d, blue). To explain such vibronic structure, we correlate the three major vibrational spacings ($v_0 - v_1 = 1087$ cm^{-1}; $v_0 - v_2 = 1559$ cm^{-1}; and $v_0 - v_3 = 2121$ cm^{-1}) with the experimental IR-spectrum for in-plane C—H bending (exp. IR 1074 cm^{-1}), symmetric phenyl ring C—C bond stretch (exp. IR 1606 cm^{-1}), and acetylenic C≡C stretching frequencies (exp. IR 2117 cm^{-1}). Such a good fit with the IR data points out on the intraligand IL($\pi\pi^*$, C≡CPh) excited state nature. Previous reports of the detailed vibronic analysis for analogous (phosphine)gold(C≡CPh) complexes support our explanations,[16,17] thus enabling us to ascribe the long-lived vibronic PL to triplet intraligand ^{3}IL($\pi\pi^*$) phosphorescence at 2.96 eV. To correlate the associated fluorescence with the ^{1}IL($\pi\pi^*$, C≡CPh) excited state, we measured PL in air to quench the dominating phosphorescence and reveal the vibronically-resolved fluorescence at 3.44 eV (excited state lifetime 5 ns, as shown in Figure 6c and Scheme 2). Note that vibronic spacing becomes less apparent after a 10 µs delay for **Au1** in a PS-film, while the PL profile resembles not only the steady-state PL (Figure 5c, black) but also the shape of phosphorescence profiles for previously reported (L)gold(I) acetylide complexes (L = phosphine and NHC-carbene).[16–19,21] All these factors further support the assignment of the long-lived phosphorescent component (Figures 5c and 6b orange and yellow) to the phosphorescence having an intraligand origin ^{3}IL($\pi\pi^*$ for C≡CPh).

The long-lived and bright ^{3}IL-phosphorescence (PLQY 43% for **Au1**) is enabled by the strong spin–orbit coupling coefficients (H_{SOC}) from the gold(I) atom and facilitated by the strong σ-donor and π-acceptor of BiCAAC-carbene ligand. We observe similar PL behavior for complex **Au2** (Figure S6, Supporting Information) and **Au3** (Figure S7, Supporting Information). The energy state diagram and various emission pathways are summarized for complex **Au1** in Scheme 2.

Transient absorption kinetic and spectra (Figure 6c,d) were measured for complex **Au1** in PS matrix to estimate the effect of the gold perturbation in promoting the intersystem crossing (ISC) rate and compare with the archetype CMA1. Complex **Au1** shows a broad excited state absorption band with little change in the spectral shape over any timescales (Figure 6d). The early-time species fully convert into a late time species on a timescale up to 9 ps for **Au1** (Figure 6c), which is somewhat shorter compared with 13 ps measured for CMA1. Faster ISC rate for complex **Au1** suggests greater contribution of the gold atom into the spin flip process compared to complex CMA1.
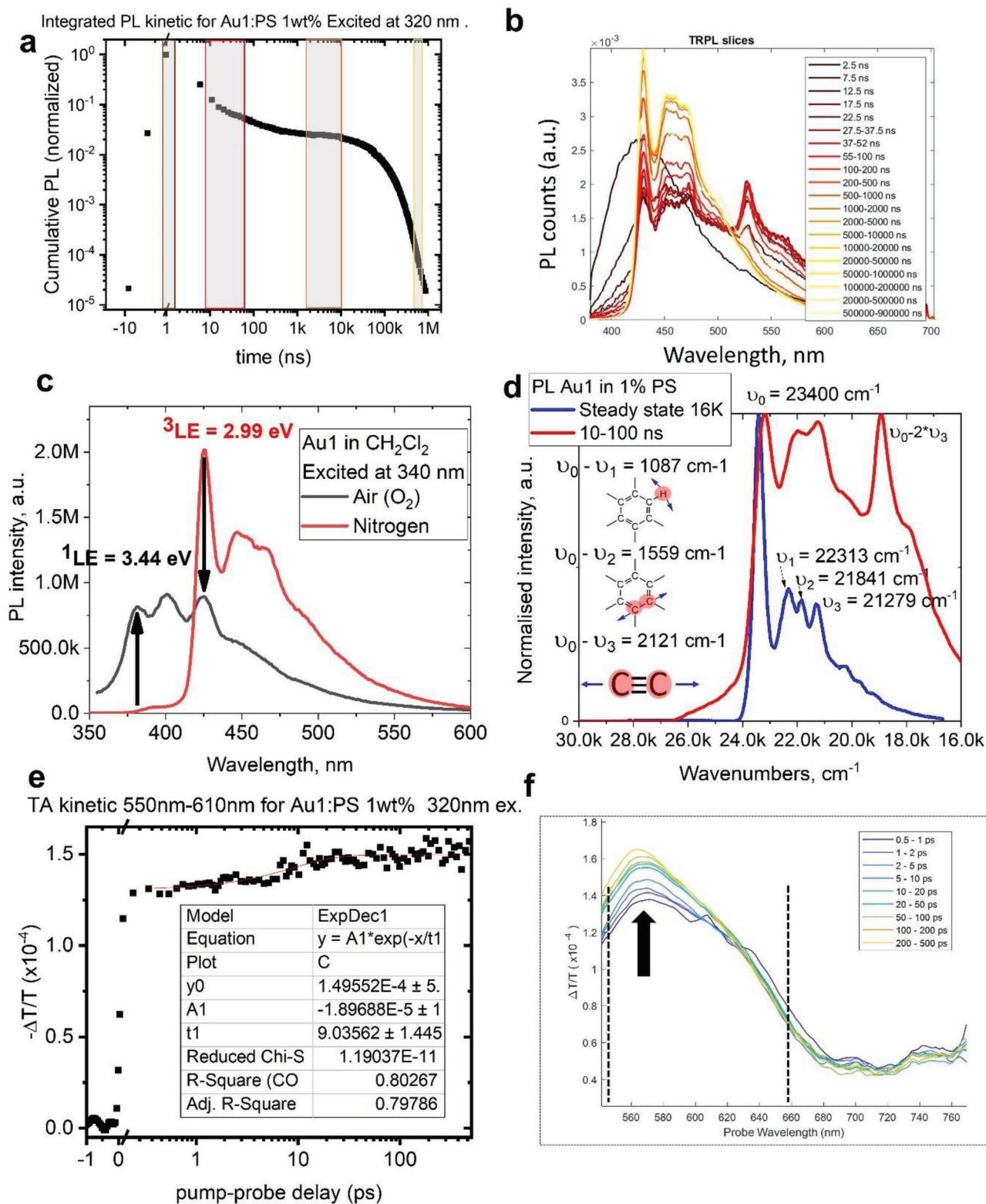
ADVANCED
SCIENCE NEWS

www.advancedsciencenews.com

ADVANCED
MATERIALS

www.advmat.de

Figure 6. Complex **Au1** in polystyrene (PS) host film (2 wt%). a) Time-resolved emission kinetics (integrated over the emission range). b) Transient photoluminescence spectra (TRPL). c) Phosphorescence quenching experiment to reveal ¹LE and ³LE states. d) Steady state phosphorescence PL at 16 K and in the range from 10 to 100 ns at 295 K with vibrational analysis. e) Transient absorption (TA) kinetic measurements with fitting parameters. f) TA spectra. Pump wavelength 320 nm.

**ADVANCED
SCIENCE NEWS**

www.advancedsciencenews.com

**ADVANCED
MATERIALS**

www.advmat.de
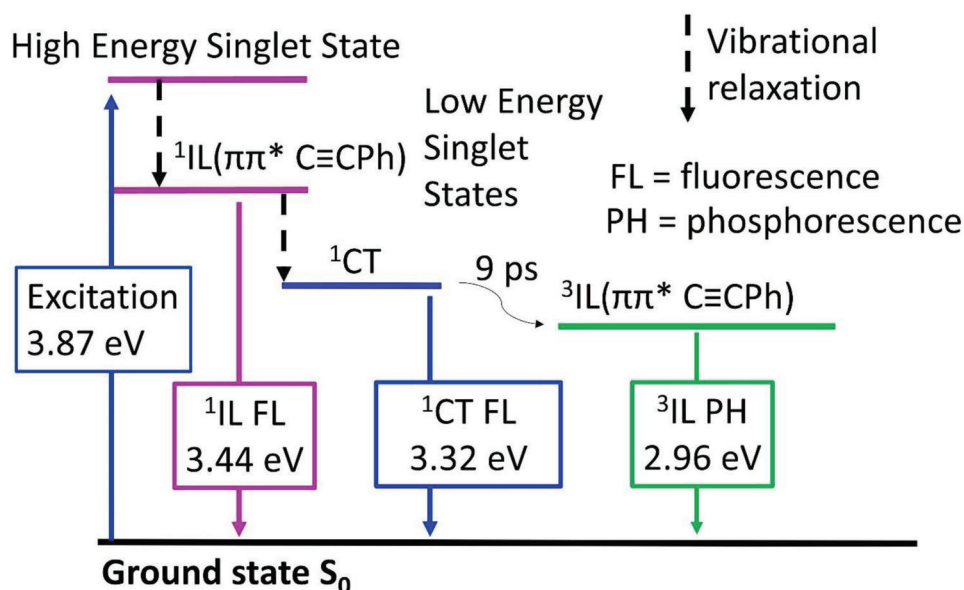
Scheme 2. Energy state diagram and emission pathways for complex **Au1** excited at 320 nm (3.87 eV).

2.3. Near-UV OLED Fabrication

Complex **Au1** demonstrated the highest energy PL with the highest PLQY up to 43% in the DPEPO host (bis[2-(diphenylphosphino)phenyl]ether oxide, **Figure 7**), indicating its suitability to test in an OLED device. To achieve a stable near UV-OLED from complex **Au1**, the electroluminescence (EL) should predominantly show the prompt-fluorescence component while minimizing the deep-blue phosphorescence component of **Au1** (Figure 6b). We proposed that it is possible to minimize the phosphorescence component via triplet energy back transfer to a host, for instance, DPEPO or PPF (**Figure 8**a). The T_1 energy level of DPEPO is reported to be 2.995 eV,[29] which is close to the T_1 energy (2.99 eV) of **Au1**. The S_1 energy for DPEPO is 3.94 eV[29] and is significantly higher than that of **Au1** ($S_1 = 3.32$ eV), thus suggesting that efficient energy transfer of the triplet excitons whereas singlet excitons could originate electroluminescence from the prompt-fluorescence (Figure 7b; and Figure S8a, Supporting Information). Indeed, when DPEPO was used as the host in the emissive layer, near-UV EL was successfully measured with high practical EQE values of 1% at 10 cd m^{-2} (Figure 7d; and Figure S8d, Supporting Information). The EQE efficiency of the first CMAc near-UV OLED is similar to those reported for organic fluorescent and TADF emitters reported for the UV-OLED (rarely exceeding 1% at practical brightness).[30]

Similarity between PL and EL-transient kinetics indicates that molecular design concepts for new CMAc emitters can be successfully translated into near-UV OLED devices. Time-resolved EL kinetics of the near-UV OLED devices from complex **Au1** (Figure 8b,c) were measured to further support the dominating fluorescence nature of the EL. The intensity of the EL reduced by 15 times within several ns after turning off the bias (Figure 8c), while the residual phosphorescence still remains in a microsecond regime. In fact, the transient EL-profiles are dominated by prompt near-UV fluorescence at 3.32 eV (orange profile, Figure 8b; and Figure S9, Supporting Information) whereas

the long microsecond decay profile demonstrates a weak phosphorescence at 2.99 eV (cyan and green profiles, Figure 8b; and Figure S9, Supporting Information). Such a weak phosphorescence profile clearly indicates that the triplet state energy can be effectively transferred to the DPEPO or PPF host. The later result indicates that such triplet exciton management can be used as a strategy to extend the OLED device operating stability—one of the major problems of the near-UV OLED on par with relatively low efficiency EQEs (rarely exceeds ≈1%). More stable near-UV OLEDs can be achieved by reducing the density of the long-lived triplet state for CMAc materials, thus reducing bimolecular quenching process at high current densities (Figure 7d) that serves as one of the major reasons for the OLED degradation.[31,32,33] A near-UV OLED device lifetime LT_{50} of ≈1 min (Figure 8d; and Table S3) was measured for **Au1** doped in DPEPO host. A more stable analog of DPEPO, such as PPF (Figure 7a) was used as a host material to further improve the operational stability in the emitting layer. Thanks to the rigid and conjugated dibenzofuran core, PPF has a slightly higher triplet energy level of 3.1 eV that was key to fabricating high efficiency PhOLEDs.[34] In fact, the device lifetime LT_{50} increased up to ≈20 min (Table S4), which is a marked improvement and the longest operating stability reported for the near-UV OLED. These exciting results demonstrate a high promise of the CMAc materials for further improvement and application in near-UV OLED devices.

The near-UV OLED generated using a neat **Au1** film as the emitting layer shows a similar emission as the PPF-host OLED (**Table 3**) and radiates with a violet-blue EL at 427 nm, due to a combination of the ^{1}IL-fluorescence and ^{3}IL-phosphorescence (Figure S10, Supporting Information). The **Au1** neat OLED device can achieve a respectable EQE of 0.7% which is likely a result of the concentration quenching that is common for phosphorescent emitters.[35] However, the very poor device stability for the neat OLED (a few seconds) clearly indicates that our triplet management approach and the use of stable PPF hosts
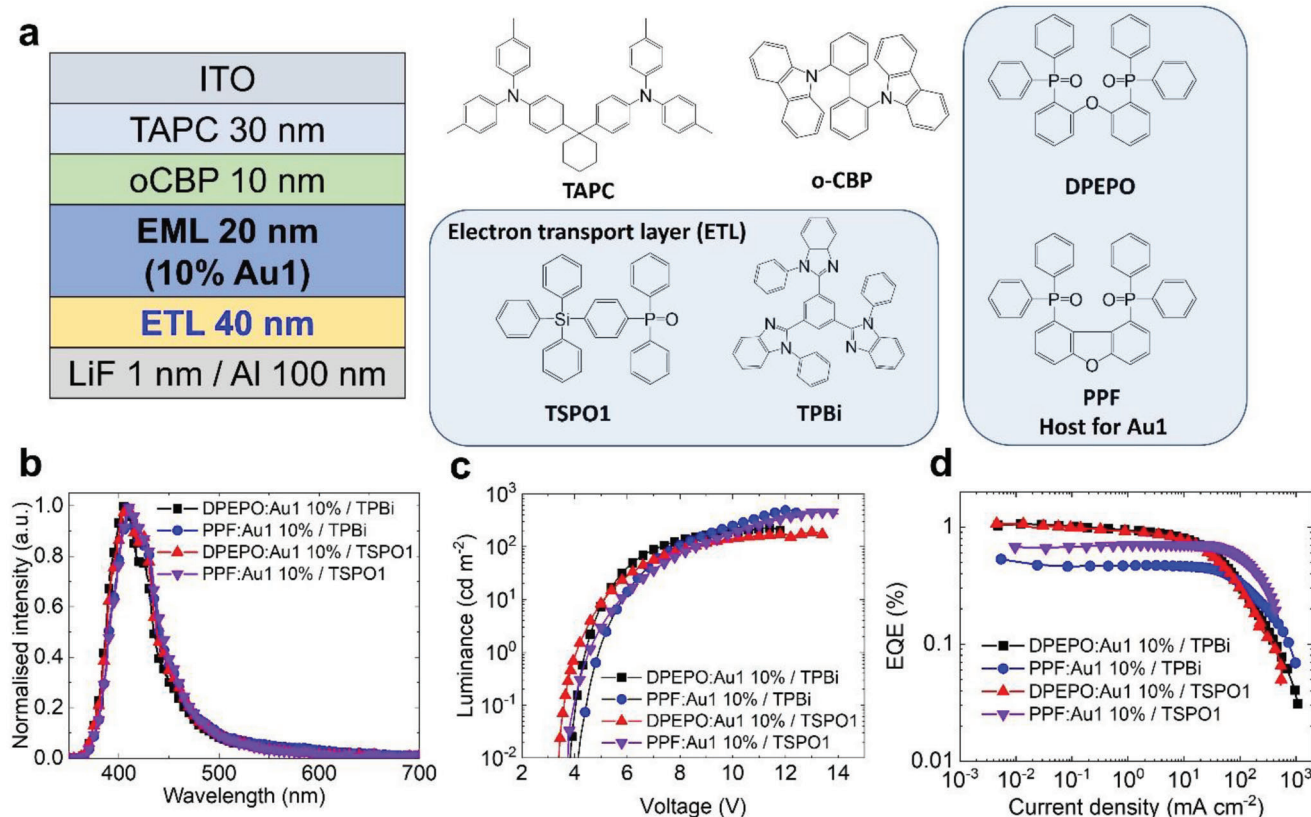
Figure 7. a) Vapor-deposited OLED device architecture based on complex **Au1** dopped in different hosts at 10% by weight and electron transport layers. b) Electroluminescence spectra of near-UV OLEDs. c) Luminance-voltage plot. d) EQE versus luminance of near UV-OLEDs in DPEPO and PPF hosts at 10% doping concentration.

is the way forward to develop future stable and efficient near-UV OLEDs.

3. Conclusion

We have successfully demonstrated a donor–acceptor molecular design strategy toward bright phosphorescent carbene—gold(I)-acetylide (CMAc) containing only carbon—gold chemical bonds. The bulky BiCAAC carbene prevented aggregation of the CMAc

molecules and enabled bright phosphorescence from 425 to 500 nm in all media with PLQY values up to 43%, which is unprecedentedly high for gold(I)acetylide complexes without aurophilic interactions. We explored the effect of an increase in substitution of the (BiCAAC)Au moieties from one to three that evoked hyperconjugation enhancing the extinction coefficients and calculated oscillator strength coefficients for complexes with multiple gold atoms **Au2** and **Au3**. The monogold complex **Au1** appeared the most efficient in the family due to

Table 3. Performance data of vapor-deposited near UV-OLEDs at 10% doping concentration of complex **Au1**.

Dopant/ETL	V_{ON} [V][a]	EQE [%]		EL_{max} [nm]	CIE [x,y][b]	LT50 @ 10 nits [min]
		max	10 cd m^{-2}			
Electron transport layer (ETL = TPBi)						
DPEPO:Au1	3.8	1.06	0.94	404	Near UV	1
PPF:Au1	4.1	0.53	0.47	410	Near UV	4
Electron transport layer (ETL = TSPO1)						
DPEPO:Au1	3.4	1.07	0.92	406	Near UV	1.5
PPF:Au1	3.7	0.71	0.70	411	Near UV	20
Neat Au1	4.6	0.81	0.72	427	Near UV	—

a) Values at brightness 0.01 cd m^{-2}. b) Commission Internationale de l'Éclairage (CIE) color co-ordinates.
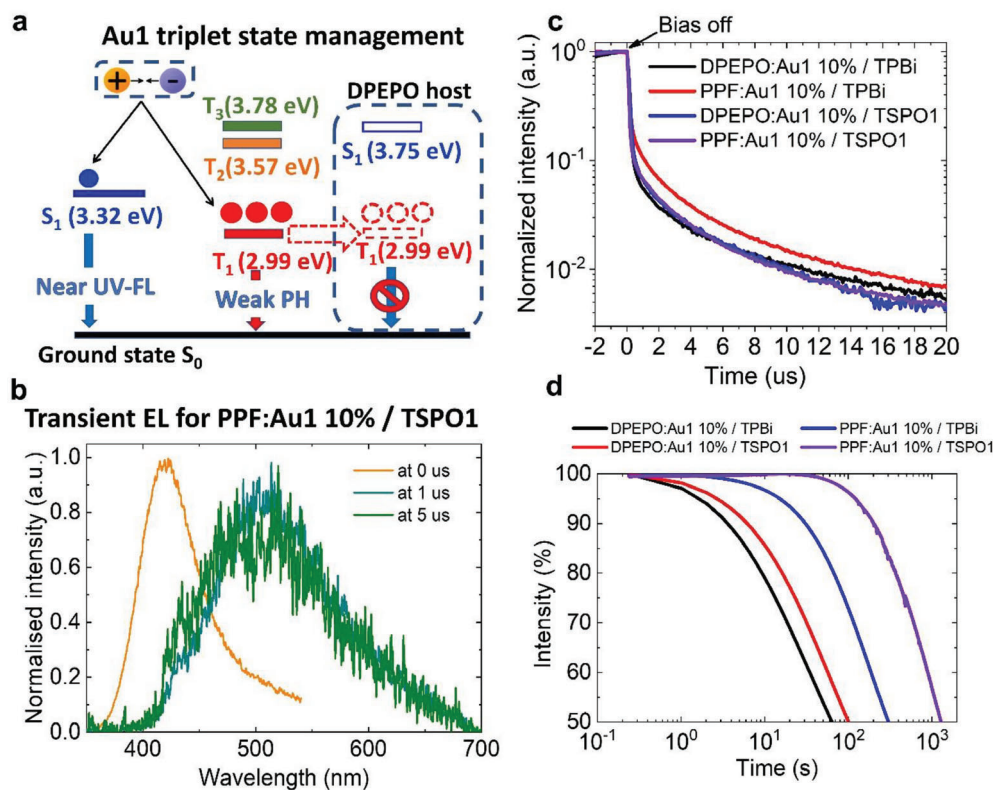
Figure 8. a) Exciton management diagram for complex **Au1** showing a triplet exciton transfer to the DPEPO host. b) Transient electroluminescence profiles for **Au1** showing strong prompt fluorescence and weak phosphorescence profile after 1 and 5 μs delays. c) Time-resolved electroluminescence (EL) decays for complex **Au1** in various near-UV OLED architectures. d) Near-UV OLED device operating lifetime curves (initial luminance 10 cd m^{-2}) at constant current under vacuum.

reduced PL quenching, which we correlate with the smaller emitter size for **Au1** and lower susceptibility to conformational changes, together with bending distortions in the triplet excited state for much larger complexes **Au2** and **Au3**. TD-DFT calculations revealed that PLQY quenching is likely associated with the bending distortions in the triplet excited state, thus directing future molecular design to minimize such distortions to enable unity PLQY phosphorescent CMAc materials. Theoretical calculations supported phosphorescence nature of the photoluminescence. The steady state and time-resolved photoluminescence from **Au1** revealed weak fluorescence ^{1}IL($\pi\pi^*$, C≡CPh) at 3.44 eV and a CT-fluorescence at 3.32 eV together with the long-lived and bright phosphorescence ^{3}IL($\pi\pi^*$, C≡CPh) at 2.96 eV. Near-UV OLED devices show respectable efficiency of up to 1% EQE at practical brightness of 10 nits from complex **Au1**. The triplet state management approach enabled selective quenching of the phosphorescent component from the **Au1** emitter by carefully choosing the host material DPEPO or PPF with an energetically similar triplet excited state. This approach proved to be an effective way of improving the device lifetimes of near-UV OLEDs, reaching up to ≈20 min, one of the longest device operational stability values among the reported for UV-OLEDs. Our new stable CMAc materials, together with the selective triplet state management approach, open a promising opportunity for realizing stable UV-OLEDs.

Supporting Information

Supporting Information is available from the Wiley Online Library or from the author.

Conflict of Interest

The authors declare no conflict of interest.

Data Availability Statement

The data that support the findings of this study are available in the Supporting Information of this article.

[1] M. Chen, Y. Liao, Y. Lin, T. Xu, W. Lan, B. Wei, Y. Yuan, D. Li, X. Zhang, *J. Mater. Chem. C* **2020**, *8*, 14665.

[2] H. W. Chen, J. H. Lee, B. Y. Lin, S. Chen, S. T. Wu, *Light: Sci. Appl.* **2018**, *7*, 17168.

[3] Y. Muramoto, M. Kimura, S. Nouda, *Semicond. Sci. Technol.* **2014**, *29*, 084004.

[4] S. Iwaguch, K. Matsumura, Y. Tokuoka, S. Wakui, N. Kawashima, *Colloids Surf., B* **2002**, *25*, 299.

[5] M. Raeiszadeh, B. Adeli, *ACS Photonics* **2020**, *7*, 2941.

[6] V. K. Sharma, H. V. Demir, *ACS Photonics* **2022**, *9*, 1513.

[7] F. Fine, P. Gervais, *J. Food Prot.* **2004**, *67*, 787.

[8] D. Lee, J. Park, W. Lee, H. S. Kim, S. Yoo, *Adv. Photonics Res.* **2021**, *2*, 2100108.

[9] J. Lin, X. Guo, Y. Lv, X. Liu, Y. Wang, *ACS Appl. Mater. Interfaces* **2020**, *12*, 10717.

[10] X. Zhang, F. You, S. Liu, B. Mo, Z. Zhang, J. Xiong, P. Cai, X. Xue, J. Zhang, B. Wei, *Appl. Phys. Lett.* **2017**, *110*, 043301.

[11] H. Zhang, G. Li, X. Guo, K. Zhang, B. Zhang, X. Guo, Y. Li, J. Fan, Z. Wang, D. Ma, B. Z. Tang, *Angew. Chem., Int. Ed.* **2021**, *60*, 22241.

[12] D. Di, A. S. Romanov, L. Yang, J. M. Richter, J. P. H. Rivett, S. Jones, T. H. Thomas, M. Abdi Jalebi, R. H. Friend, M. Linnolahti, M. Bochmann, D. Credgington, *Science* **2017**, *356*, 159.

[13] A. L. Allred, *J. Inorg. Nucl. Chem.* **1961**, *17*, 215.

[14] V. W. W. Yam, V. K. M. Au, S. Y. L. Leung, *Chem. Rev.* **2015**, *115*, 7589.

[15] M. C. Tang, M. Y. Chan, V. W. W. Yam, *Chem. Rev.* **2021**, *121*, 7249.

[16] V. W. W. Yam, S. W. K. Choi, *J. Chem. Soc. Dalton Trans.* **1996**, *22*, 4227.

[17] H.-Y. Chao, W. Lu, Y. Li, M. C. W. Chan, C.-M. Che, K.-K. Cheung, N. Zhu, *J. Am. Chem. Soc.* **2002**, *124*, 14696.

[18] G. C. Fortman, A. Poater, J. W. Levell, S. Gaillard, A. M. Z. Slawin, I. D. W. Samuel, L. Cavallo, S. P. Nolan, *Dalton Trans.* **2010**, *39*, 10382.

[19] J. A. Garg, O. Blacque, J. Heier, K. Venkatesan, *Eur. J. Inorg. Chem.* **2012**, *11*, 1750.

[20] A. A. Penney, G. L. Starova, E. V. Grachova, V. V. Sizov, M. A. Kinzhalov, S. P. Tunik, *Inorg. Chem.* **2017**, *56*, 14771.

[21] F.-H. Yu, X.-F. Song, G.-H. Liu, X. Chang, K. Li, Y. Wang, G. Cui, Y. Chen, *Chem. – Eur. J.* **2022**, *28*, e202202439.

[22] F. Chotard, V. Sivchik, M. Linnolahti, M. Bochmann, A. S. Romanov, *Chem. Mater.* **2020**, *32*, 6114.

[23] J. Vicente, M. T. Chicote, M. M. Alvarez-Falcón, P. G. Jones, *Organometallics* **2005**, *24*, 5956.

[24] C. M. Cardona, W. Li, A. E. Kaifer, D. Stockdale, G. C. Bazan, *Adv. Mater.* **2011**, *23*, 2367.

[25] S. Montanaro, D. G. Congrave, M. K. Etherington, I. A. Wright, *J. Mater. Chem. C* **2019**, *7*, 12886.

[26] A. Gutiérrez-Blanco, V. Fernández-Moreira, M. C. Gimeno, E. Peris, M. Poyatos, *Organometallics* **2018**, *37*, 1795.

[27] W. Wang, Y. Hong, X.g Shi, C. Minot, M. A. Van Hove, B. Z. Tang, N. Lin, *J. Phys. Chem. Lett.* **2010**, *1*, 2295.

[28] T.-Y. Li, D. Sylvinson, M. Ravinson, R. Haiges, P. I. Djurovich, M. E. Thompson, *J. Am. Chem. Soc.* **2020**, *142*, 6158.

[29] J. Zhang, D. Ding, Y. Wei, H. Xu, *Chem. Sci.* **2016**, *7*, 2870.

[30] Y. Luo, S. Li, Y. Zhao, C. Li, Z. Pang, Y. Huang, M. Yang, L. Zhou, X. Zheng, X. Pu, Z. Lu, *Adv. Mater.* **2020**, *32*, 2001248.

[31] C. S. B. Matthews, A. S. Romanov, N. C. Greenham, *J. Mater. Chem.* **2022**, *10*, 14180.

[32] J. Lee, C. Jeong, T. Batagoda, C. Coburn, M. E. Thompson, S. R. Forrest, *Nat. Commun.* **2017**, *8*, 15566.

[33] N. C. Giebink, B. W. D'Andrade, M. S. Weaver, P. B. Mackenzie, J. J. Brown, M. E. Thompson, S. R. Forrest, *J. Appl. Phys.* **2008**, *103*, 44509.

[34] P. A. Vecchi, A. B. Padmaperuma, H. Qiao, L. S. Sapochak, P. E. Burrows, *Org. Lett.* **2006**, *8*, 4211.

[35] S. Reineke, M. A. Baldo, *Phys. Status Solidi A* **2012**, *209*, 2341.